2nd Advanced Optical Metrology Compendium

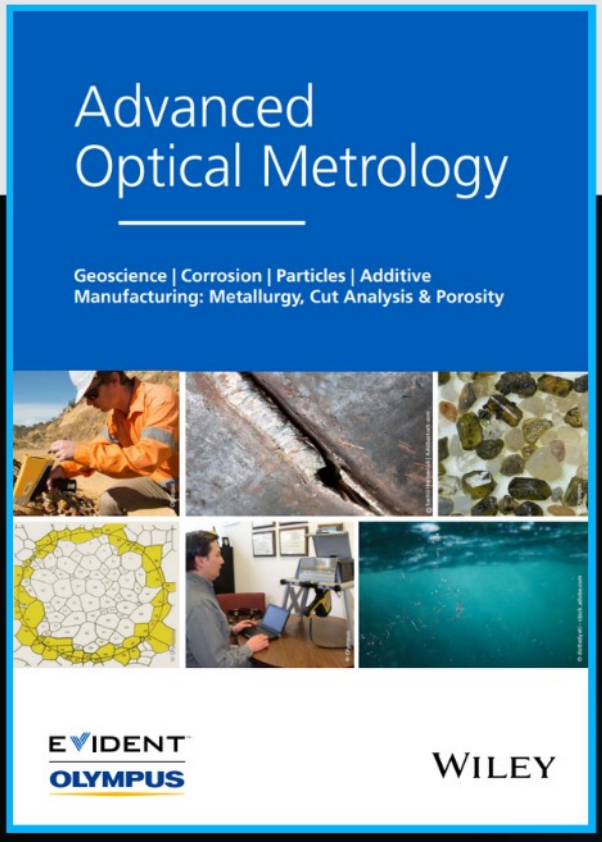

The latest eBook from Advanced Optical Metrology. Download for free.

This compendium includes a collection of optical metrology papers, a repository of teaching materials, and instructions on how to publish scientific achievements.

With the aim of improving communication between fundamental research and industrial applications in the field of optical metrology we have collected and organized existing information and made it more accessible and useful for researchers and practitioners.

EVIDENT
OLYMPUS

WILEY

ADVANCED FUNCTIONAL MATERIALS
www.afm-journal.de

Robust Single-Walled Carbon Nanotube-Infiltrated Carbon Fiber Electrodes for Structural Supercapacitors: from Reductive Dissolution to High Performance Devices

Evgeny Senokos, David B. Anthony, Noelia Rubio, Maria Crespo Ribadeneyra, Emile S. Greenhalgh, and Milo S. P. Shaffer**

Multifunctional electrodes for structural supercapacitors are prepared by vacuum infiltration of single-walled carbon nanotubes (SWCNTs) into woven carbon fibers (CFs); the use of reductive charging chemistry to form nanotubide solutions ensured a high degree of individualization. The route is highly versatile, as shown by comparing four different commercial nanotube feedstocks. In film form, the pure nanotubide networks ("bucky-papers") are highly conductive (up to 2000 S cm^{-1}) with high surface area (>1000 m^2 g^{-1}) and great electrochemical performance (capacitance of 101 F g^{-1}, energy density of 27.5 Wh kg^{-1} and power density of 135 kW kg^{-1}). Uniformly integrating these SWCNT networks throughout the CF fabrics significantly increased electrical conductivity (up to 318 S cm^{-1}), surface area (up to 196 m^2 g^{-1}), and in-plane shear properties, all simultaneously. The CNT-infiltrated CFs electrodes exhibited intrinsically high specific energy (2.6–4.2 Wh kg^{-1}) and power (6.0–8.7 kW kg^{-1}) densities in pure 1-ethyl-3-methylimidazolium bis(trifluoromethylsulfonyl)imide (EMIM TFSI) electrolyte. Multifunctional structural supercapacitors based on CNT-coated CFs offer a substantial increase in capacitive performance while maintaining the tensile mechanical properties of the as-received CF-based composite. This non-damaging approach to modify CFs with highly graphitic, high surface area nanocarbons provides a new route to structural energy storage systems.

1. Introduction

The electrification of the transport sector offers a promising route to alleviating environmental burdens, particularly from greenhouse gases, but also other harmful emissions.[1] One of the central challenges is the need for an effective electrical energy storage system since the masses of such systems are significant and feed back into the overall energy requirements for the vehicle. In the automotive sector, the performance of the battery system affects range and user acceptance. In aerospace, the sensitivity to mass is even greater, and the available energy storage density will determine the format of future all-electric aircraft.[2] Extensive efforts are underway to improve the absolute performance of supercapacitor and battery systems; although commercial systems have improved steadily, the gains are relatively modest.[3] Multifunctional devices that combine structural properties with electrochemical energy storage provide a more radical route to improving the

E. Senokos, D. B. Anthony, N. Rubio, M. S. P. Shaffer
Department of Chemistry
Imperial College London
82 Wood Lane, White City Campus, London W12 0BZ, UK
E-mail: evgeny.senokos@mpikg.mpg.de; m.shaffer@imperial.ac.uk
N. Rubio
Department of Organic and Inorganic Chemistry
University of Alcalá
Madrid 28802, Spain

The ORCID identification number(s) for the author(s) of this article can be found under https://doi.org/10.1002/adfm.202212697.

DOI: 10.1002/adfm.202212697

M. C. Ribadeneyra
School of Materials Science and Engineering
Queen Mary University of London
Mile End Road, London E1 4NS, UK
M. C. Ribadeneyra
Department of Chemical Engineering
Imperial College London
South Kensington Campus, London SW7 2AZ, UK
E. S. Greenhalgh
Department of Aeronautics
Imperial College London
South Kensington Campus, London SW7 2AZ, UK
M. S. P. Shaffer
Department of Materials
Imperial College London
South Kensington Campus, London SW7 2AZ, UK

performance, even to the point of effectively "massless" energy storage.[4,5] Although they offer greater technical challenges, systems based on multifunctional materials are, in principle, more effective than multifunctional structures that simply embed conventional batteries, since the same atoms can serve multiple functions.

The development of multifunctional systems fulfilling both structural and electrochemical energy storage roles has been previously shown to offer system-level weight and volume reductions.[4–6] This concept has been widely explored in batteries,[7–10] supercapacitors,[11–13] dielectric capacitors,[14–17] fuel cells[18,19] as well as sensors[20,21] and actuators.[22–24] In particular, the study of structural supercapacitors has gained recent interest, due to their long lifetime, dimensional stability, and relative environmental tolerance.[25–27] Supercapacitors are promising for a wide spectrum of applications with high power and long cycle stability requirements, including backup power and load management schemes, in partnership with batteries.[28,29] Most supercapacitors are electrochemical double-layer capacitors (EDLCs), though often augmented by redox-active elements to form pseudo-capacitors or hybrid systems.[30]

Carbon fibers (CFs) have exceptional mechanical properties and high inherent electrical conductivity, which underpins their widespread use as a reinforcement in structural composites,[31,32] as well as interest in their use as a conductive scaffold in electrochemical energy storage systems.[33,34] Whilst small fiber-scale devices have been explored, most multifunctional structural supercapacitor composites have a layered architecture mirroring that of both structural laminates and most electrochemical devices. The simplest embodiment consists of two conductive structural CF electrodes, separated by a structural insulating spacer and infused with an ionically conductive matrix. Each component plays a crucial role, simultaneously providing sufficient electrochemical and mechanical contributions to realize an entire structural power device capable of offering weight/volume reduction at a system level.

The main intrinsic limitation to using CFs in structural supercapacitors is their low specific surface area (≈0.2 $m^2\ g^{-1}$) since EDLC energy storage is defined by the charge accumulating at the electrode-electrolyte interface. In the context of multifunctional systems, the external surface area must be maximized without compromising the mechanical properties of the material.

Earlier studies have explored chemical activation of CFs,[35] direct growth of carbon nanotubes[36] and graphene nanoflakes on CFs,[27] deposition of inorganic transition oxide-based nanostructures[37,38] and embedding CFs in a continuous network of carbon aerogel (CAG).[25,36] Integration of a highly porous monolithic CAG (>700 $m^2\ g^{-1}$) has shown to be a successful approach, leading to up to 100-fold increase in capacitance, while providing good shear modulus (895 MPa) and shear strength (8.7 MPa) in the matrix.[25] The main drawback of the CAG modification method is associated with the high temperature (>800 °C) required to convert the organic gel precursor into the conductive high surface area carbon network. This step may degrade the CFs mechanical properties, as has also been observed for high-temperature growth of nanocarbons on the surface of CFs.[27,39] On the other hand, a lower pyrolysis temperature reduces the degree of carbonization of the CAG, the associated electric conductivity, and ultimately, the power performance of the electrodes. Therefore, there is a particular interest in a low-temperature approach to CF modification with highly conductive and large surface area materials.

Previous studies have explored the use of unidirectional, non-woven, CNT fiber veils impregnated with polymer electrolytes as interleaves between CF plies in multifunctional composites.[26] CNT fiber veils offer good electrochemical performance and enable additional interlaminar toughening of the structural composite. Furthermore, mechanical properties of the structural system can be further improved by machining coarse holes through the structure, filled with structural epoxy to transfer load, but at the expense of reducing the mass loading of active material. However, in this architecture, the electrically active CNT veil is inserted into the lay-up, increasing mass and volume; the surfaces of the individual CFs and the volume within the CF plies are effectively unused. An alternative strategy, therefore, is to deposit nanocarbon dispersions within the plies, effectively utilizing the full structural electrode volume. The crucial factor for uniform coverage of the internal fabric structure is compatibility of the nanocarbon dispersion with the hydrophobic surface of CFs. Aqueous dispersions of CNTs are often prepared by surfactant-assisted sonication or aggressive chemical oxidation.[40] However, these approaches tend to shorten and damage the graphitic CNT structure, as well as introduce unwanted contamination, limiting both mechanical and electrochemical performance. As an alternative to these damaging routes, nanocarbons can be charged, by chemical reduction, to form thermodynamically-stable solutions of individual, undamaged species.[41] Such solutions of negatively-charged CNT anions ("nanotubides") are easily manipulated and can be assembled in a variety of architectures to form highly graphitized and large surface area materials.[42–44] In addition, the charge can be used deliberately to initiate a wide spectrum of functionalization and grafting reactions.[45,46]

This paper explores a new approach to producing large surface areas and highly conductive electrodes, using reductive chemistry to infiltrate highly individualized SWCNTs into CF fabrics. The room temperature method allows a highly conductive (up to 2000 S cm^{-1}) and high surface area (>1000 $m^2\ g^{-1}$) network of SWCNTs to be introduced within the CF plies, maximizing electrochemical performance, without increasing the volume of the composite or degrading the intrinsic CF properties. The reductive dissolution method maximizes the degree of SWCNTs individualization, and hence the accessible surface area, in the final hybrid electrode. Since the approach can be applied to most nanocarbon feedstocks, the properties can be manipulated by selecting CNT starting materials with different dimensions, perfection, and purity. This study explores the infiltration of a range of commercial SWCNTs into CFs to identify the characteristics that offer the best multifunctional performance for use in composite-based structural supercapacitors.

2. Results and Discussion

SWCNT-modified CFs electrodes were prepared by vacuum-assisted infiltration of highly individualized nanocarbon

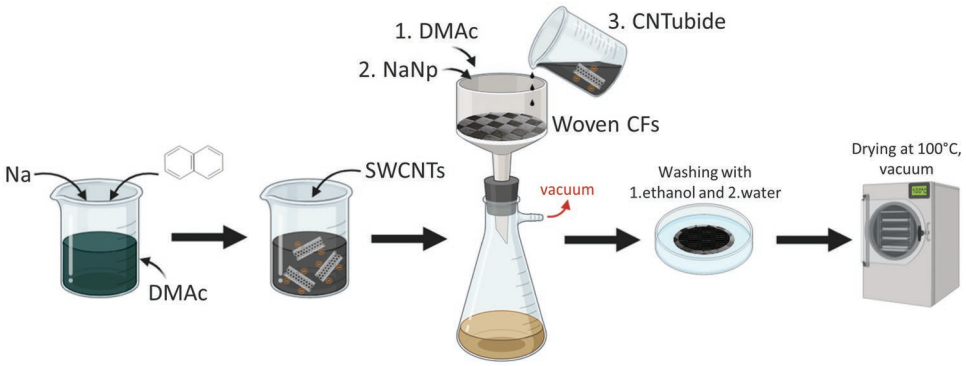

Figure 1. Schematic of the fabrication of SWCNT-infiltrated CF-based structural electrodes.

dispersions into pre-washed fabrics of CFs, as shown schematically in **Figure 1**. Reference buckypapers were prepared by filtration directly onto the filter membrane in the absence of the CF fabric. The SWCNTs were dispersed in an organic solvent (DMAc) by forming negatively charged carbon nanotubide (CNTubide) ions using sodium naphthalide as a reducing agent.[47]

CNT characteristics, including length, aspect ratio, degree of graphitization, specific surface area, and purity, influence both intrinsic properties, such as electrical conductivity, and the performance once assembled into a network. Four types of SWCNTs obtained from different suppliers were selected for infiltration onto the CF fabrics: HiPco, Tuball, Supergrowth, and EDIPS. Each type of SWCNT material offers a specific advantage: short length (<1 µm) HiPco provides better dispersibility and good specific surface area (SSA), long and highly graphitized Tuball and EDIPS exhibit high electrical conductivity (500-2000 S cm^{-1}) and mechanical properties, more defective Supergrowth shows large SSA (>1000 m^2 g^{-1}) and capacitance (101 F g^{-1}). All four materials exhibit great energy storage performance with measured energy density in the range of 13.5–27.5 Wh kg^{-1} and specific power of 75–135 kW kg^{-1}. These properties are exceptionally high for buckypapers, reflecting the effectiveness of the reductive dissolution process, and providing a high degree of individualization of undamaged, high aspect ratio SWCNTs.[44,48–51] The properties measured for the reference buckypapers prepared by reductive processing are presented in Table S1 and Figure S2 (Supporting Information), alongside selected manufacturers' data for the SWCNT starting powders. Spread tow CF fabrics improve the mechanical performance of composites, by both increasing fiber alignment and reducing the tendency for delamination; they are also attractive for structural supercapacitors, as they should reduce ionic diffusion distances, and allow a larger number of cells to be stacked in series within a given volume.[52]

As-received SWCNTs were dispersed at a concentration of 1 mg ml^{-1} and filtered through woven spread tow CF fabric. The total mass loading of CNTs for all four samples was maintained around 0.9 mg cm^{-2}, corresponding to 17 wt.% of the total electrode mass. The SWCNT concentration was selected to be just below the rheological percolation threshold, in order to minimize viscosity and encourage infusion. The loading was estimated to fill the void space within the CF fabric, assuming a network density ≈150 mg ml^{-1}; whilst higher densities form after drying, infusion is limited by the wet gel concentration.[44] To remove any chemicals from the CF surface that could potentially quench the charge of the CNTubide during infiltration (e.g., binder or size), the CFs were prewashed with pure DMAc and NaNp solution prior to nanotubide infiltration. The wash with NaNp may charge the fibers, helping to prevent premature adsorption of the negatively-charged nanotubide, via coulombic repulsion, hence facilitating its infiltration throughout the fabric.

The optical and SEM images of the infused fabrics, after washing and drying, show the presence of CNTs on both upper and lower surfaces, confirming that they can easily pass through the gaps between the carbon fibers (Figure 1a,d; Figure S3, Supporting Information). After drying, the CNTs act as sizing, preventing individual desized CF filaments from becoming damaged or misaligned, during subsequent handling; without this behavior, the removal of the original size during the solvent washing would complicate composite fabrication.[53] SEM showed uniform coverage of SWCNTs on the surface of the fabrics (**Figure 2**e; Figure S4, Supporting Information) and on the individual fibers (Figure 2f,g), in sharp contrast to the bare, as-received CFs which exhibited only faint crenulations and no nanofibrous features (Figure 2b,c). The CNTs form a well-dispersed network (Figure 2g) both at a macroscopic level on the surface of the woven fabrics and at a microscale on the surface of the individual CFs (Figure 2h). The CFs lying on the external surface of the fabric are embedded into a networked nanocarbon layer, similar to a buckypaper or a veil (Figure S5, Supporting Information). At the same time, throughout the thickness of the fabric, the surfaces of the individual CFs are covered with a thin CNT coating (Figure 2h). This architecture is formed during self-filtration of SWCNTs on the bottom of the fabric which increases the gel concentration around CFs (see schematic in Figure S6, Supporting Information). The infiltration continues until a layer of SWCNTs forms on top of the fabric, indicating that the space between the fibers is filled with SWCNT gel. On subsequent drying, the surface tension causes the nanotubide gel to contract and densify, forming a buckypaper-like structure at the top and bottom of the fabric. Within the fabric, the constraint provided by the CF causes the gel to collapse onto the fiber surfaces, forming a connected, buckypaper-like network wrapped around all the fibers.

In all cases, the SWCNT mass loading was around 17 wt.% of the total mass of the hybrid fabric; filtration losses were

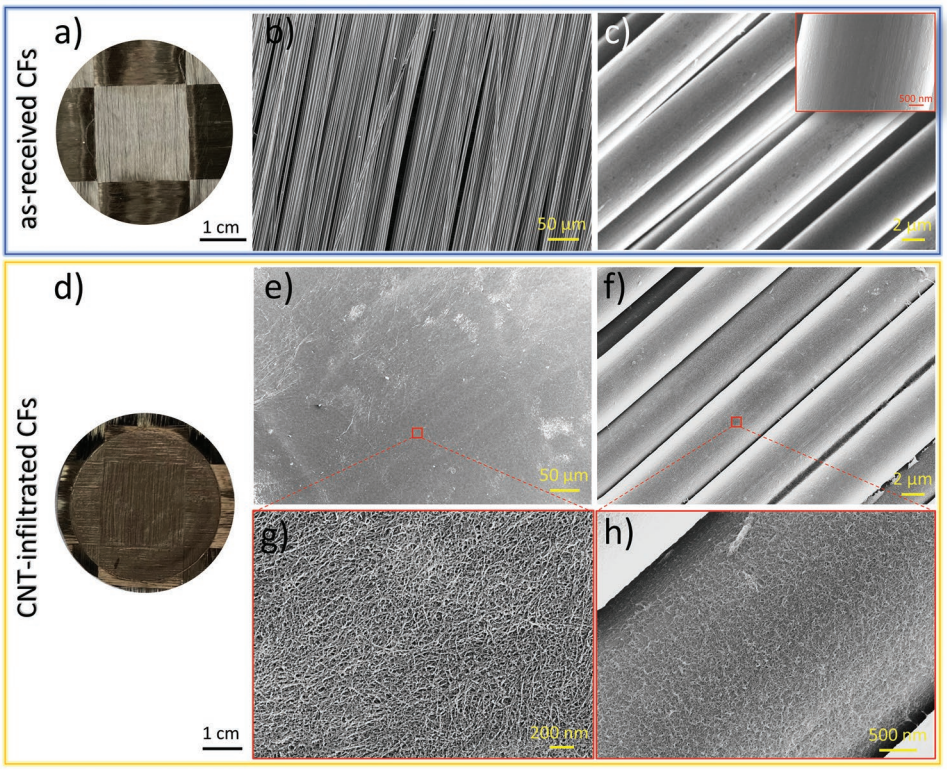

Figure 2. a–c) Optical and scanning electron microscopy (SEM) images of as-received and d–h) Supergrowth CNT-infiltrated CFs. b,e,g) The second column illustrates the top surface morphology of the fabric (i.e., external surface), c,f,h) whilst the third column shows the surface of the individual CFs (i.e., inner surface).

negligible. This increase in the fabric mass is modest and will be even less significant in the final composite, as the SWCNTs will displace the resin phase (depending on the structural electrolyte chosen, the resin density may be higher or lower than the SWCNTs themselves). Nevertheless, this small addition of SWCNTs has a dramatic effect on surface area. The results of nitrogen gas physisorption analysis (Figure S7, Supporting Information) showed that infiltration of SWCNTs into CFs produced up to three orders of magnitude larger SSA as compared to that of as-received CFs, reaching up to 196 $m^2\ g^{-1}$ for the roughest, Supergrowth nanotubes (see Table S3). Given that the mass loading of SWCNTs is only 17 wt.%, this average surface area or the SWCNT-CF hybrid translates to a surface area of 1152 $m^2\ g^{-1}$ normalized to the mass of the nanotubes themselves; in other words, approaching the value of 1315 $m^2\ g^{-1}$ for the external surface of perfectly isolated SWCNTs. Considering that the SWCNTs are adsorbed on the CFs surface and partially networked in small bundles, such a high value for the Supergrowth nanotubes likely reflects access to the internal surface through the wall pores or broken ends, as shown by the strong peak in the pore size distribution around 1 nm (Figure S7c, Supporting Information). The other three SWCNT hybrids have around half the surface area, and a much smaller micropore fraction, indicating mainly closed nanotubes, with a low degree of bundling. All the samples exhibited mesopores in the 10–40 nm range consistent with the gaps in the porous SWCNT network (as visualized by SEM in Figure 2g); the exact size varied with tube type, presumably depending on the influence of SWCNT diameter and stiffness on network packing.

Raman spectroscopy (**Figure 3**) demonstrated a significant increase in graphiticity following SWCNT deposition, as expected given the more crystalline structure of SWCNTs compared to CFs. The spectra of all four infiltrated fabrics (Figure 3a) showed the characteristic SWCNT bands: D- (1340 cm^{-1}), G- (1570 cm^{-1}), and 2D-modes (2688 cm^{-1}), as well as the low-frequency radial breathing modes (RBM) between 100–300 cm^{-1}. The peak intensity of the D-mode can be used as an estimate of graphitic defects, and the intensity ratio of the D-mode to the G-mode (I_D/I_G) can be used as a measure of the quality of the samples (e.g., quantity of structural defects or/and amount of amorphous carbon). Overall, infiltration of SWCNTs considerably reduced I_D/I_G ratio of the as-received CFs from 0.87 to 0.01–0.16 as confirmed by Raman mapping over >5000 μm^2 regions and 130 independent points, statistically represented in normalized histograms (Figure 3b). The high I_D/I_G for CFs is typical, related to large sp^3 carbon content, or incomplete graphitization.[54,55] Deposition of relatively crystalline EDIPS and Tuball SWCNTs led to a more pronounced reduction of I_D/I_G (0.011 ± 0.001 and 0.015 ± 0.002, respectively), as compared to HiPco and Supergrowth nanotubes (0.087 ± 0.002 and 0.159 ± 0.008, respectively). The low I_D/I_G reflects both the presence of highly graphitic SWCNTs and the non-damaging nature of the reductive dissolution approach.[47]

Since the penetration depth of the Raman probe is smaller than the thickness of the CNT layer on the fabrics (typically

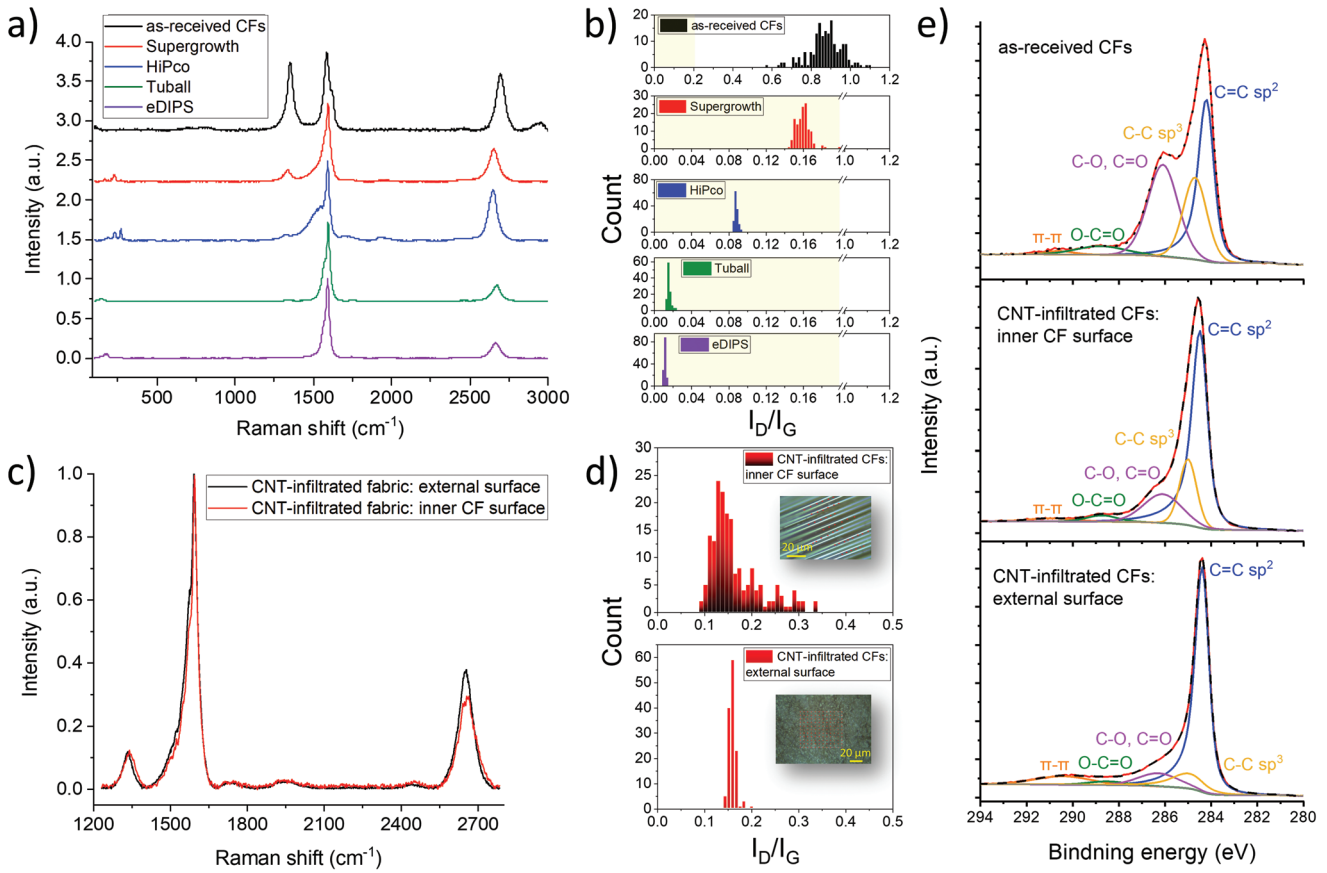

Figure 3. a) Raman spectra and b) normalized histograms of Raman D/G intensity ratios for the as-received and CNT-infiltrated CF samples; c) Raman spectra, d) Raman mapping histograms of D/G intensity ratios and e) C1s XPS spectra comparing external top layer and inner CF layer (surface of individual filaments) of Supergrowth CNT-infiltrated fabrics.

90% of the Raman signal originates from the 50 nm depth),[56] Raman spectra were additionally obtained from the internal region of the fabrics. All the spectra, from both the external and inner surfaces of the modified fabrics (Figure 3c), exhibited similar features, including the characteristic asymmetric G peak and low intensity of D band, confirming the presence of SWCNTs throughout the fabric (Figure 3d).

The deposition of highly graphitic nanocarbons was also established by X-ray photoelectron spectroscopy (XPS) analysis. The C1s XPS spectrum of the CNT-infiltrated CFs (Figure 3e) exhibited a dominant contribution of sp^2 C=C carbon (284.4 eV) and increased intensity of the $\pi-\pi$ signal (290.5 eV) as compared to the unmodified CFs. The as-received, commercially electro-oxidized fibers showed a significant oxygen content (C—O, C=O at 286.3 eV and O—C = O at 288.6 eV) and sp^3 C—C carbon (285.0 eV) manifested in the doublet C1s feature and the asymmetry of the main peak. After SWCNT infiltration, the observed oxygen content was reduced from 30.6 at% to 7.5 at% for the external surface of the hybrid fabric, and to 14.1 at.% in the interior. Quantitative analysis data are presented in Table S2 and Figure S8 in Supporting Information. The C1s peak collected from the interior of the fabric resembled the shape of C1s signal for SWCNTs, with only a small contribution from the non-graphitic components associated with the CFs.

The advantages of using the reductive dissolution to prepare the CNT dispersions for CF fabric infiltration were illustrated by comparison with a conventional SWCNT bath sonicated approach. Bath sonication produced a relatively poor, unstable SWCNT dispersion that did not readily infiltrate into the fabric. Instead, an inhomogeneous CNT coating is formed predominantly on top of the CFs which increased the thickness of the hybrid material. An increase in I_D/I_G ratio values in the Raman spectra additionally confirmed the damaging effect of bath sonication on the graphitic structure of CNTs (Figure S9, Supporting Information).

The presence of the highly graphitic SWCNTs significantly increased the in-plane electric conductivity of the infiltrated CF fabrics, a critical factor for current collection in structural power devices. The conductivity values, measured by the four-point probe setup, are listed in Table S3 (see Supporting Information). The highest conductivities were provided by EDIPS (317 ± 15 S cm^{-1}) and Tuball (287 ± 21 S cm^{-1}) SWCNTs, showing a good correlation with the CNTs quality (i.e., high aspect ratio and low defect density favor conductivity). For comparison, the CFs coated with bath-sonicated Tuball SWCNTs had less than half the electrical conductivity (110.4 ± 9.6 S cm^{-1}). CFs modified with the less graphitized Supergrowth (79 ± 13 S cm^{-1}) and HiPco (151 ± 6.9 S cm^{-1}) SWCNTs had lower conductivities but

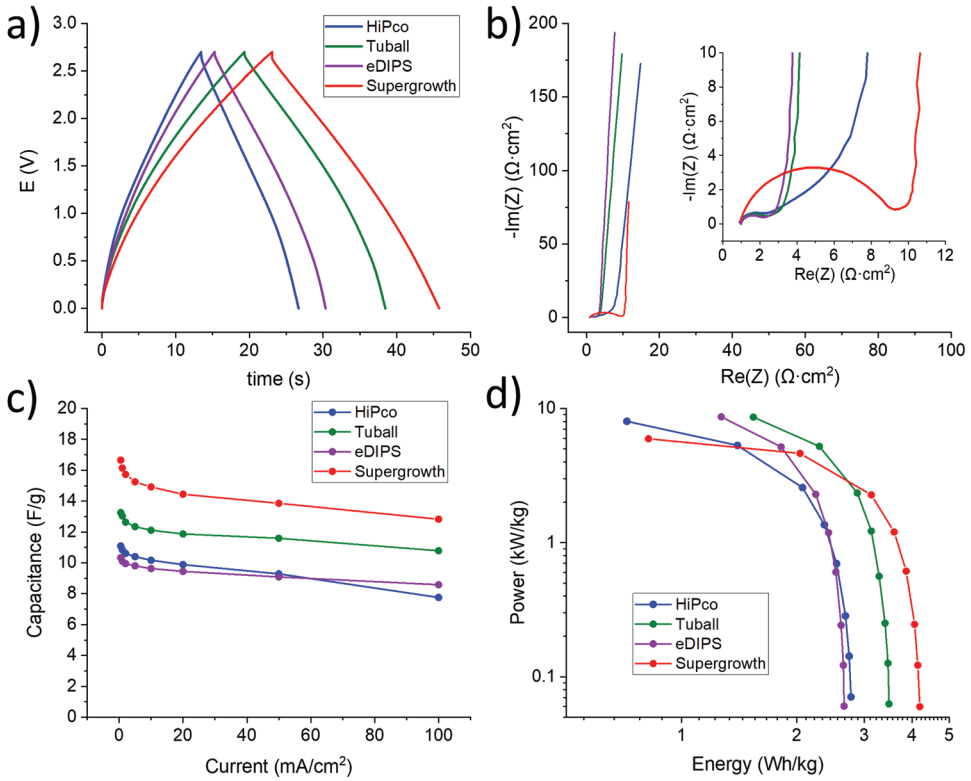

Figure 4. Electrochemical performance of CNT-infiltrated CFs electrodes in a full cell: a) GCD profiles, b) Nyquist plots, c) specific capacitance and d) Ragone plots.

still a considerable enhancement compared to the non-modified CF fabric (5.2 ± 0.1 S cm^{-1}).

Prior to assembling a full cell structural multifunctional device, the intrinsic capacitances of the hybrid electrodes were evaluated in a conventional liquid electrolyte system. This purely electrochemical characterization is often omitted from the structural energy storage field, but it is important to understand and compare the intrinsic properties of the electrodes.[57] The electrochemical performance of CNT-infiltrated CFs was evaluated in a 2-electrode symmetric Swagelok cell setup using 1-ethyl-3-methylimidazolium bis(trifluoromethylsulfonyl)imide (EMIM TFSI) ionic liquid electrolyte. The negligible SSA and hence EDLC contribution of the CFs makes it difficult to display the performance of the non-modified fabrics relative to the CNT-infiltrated electrodes; however, the CNT-infiltrated hybrids showed a strong energy storage response. The galvanostatic charge-discharge (GCD) curves exhibited bulging profiles (**Figure 4**a) as opposed to the conventional triangular shape of EDLCs. However, this behavior is well-known in the field and is attributed to the quantum capacitance of low dimensional CNTs with a finite density of states near the Fermi level, which manifests in a non-linear dependence between the charge and the potential applied.[58–60] The small ohmic drop indicates a low equivalent series resistance (ESR, combination of bulk electrolyte and electrode intrinsic resistances) of the devices, attributed to the high electrical conductivity and accessible pore structure.

Electrochemical impedance data show consistent trends. Nyquist plots (Figure 4b) exhibited similar ESR values ≈2.2 Ωcm^2 for the assembled cells, with a slightly increased resistance for the least conductive Supergrowth CNT-based electrodes (ESR = 9.5 Ωcm^2). A vertical line at low frequency suggests nearly ideal EDLC behavior with no indication of the diffusion control region, typically observed in impedance loci as a slope of $\pi/4$ (45°). The direct transition from purely resistive behavior (phase angle ≈0°) to nearly pure capacitive response (phase angle 85–87°) demonstrates excellent pore accessibility excluding any diffusion limitations caused by pore size or shape. However, small alterations were observed for the device assembled with HiPco SWCNTs, showing an inclined line in the mid-frequency range. This feature can be related to minor ion diffusion limitations associated with more tightly packed, small-diameter, short HiPco SWCNTs, which became more evident at higher nanotube loadings (Figure S10, Supporting Information). The relaxation time constant, the time required to release 50% of the total stored energy of the EDLC, was estimated to be 30–200 ms. These values are considerably smaller than those for both activated carbon electrodes employed in conventional supercapacitors (260–1250 ms)[61,62] and CAG-modified CFs (2.5 s),[52] reflecting the high conductivity of the SWCNT networks and indicating a higher power performance for the hybrid SWCNT/CF fabrics. More details of EIS analysis of the tested devices are presented in Figure S11 (Supporting Information).

The specific capacitance was calculated from the GCD discharge curves (Figure 4c). The difference in capacitance for four types of SWCNTs followed the trend in measured SSA. The fabrics infiltrated with Supergrowth SWCNTs gave the largest

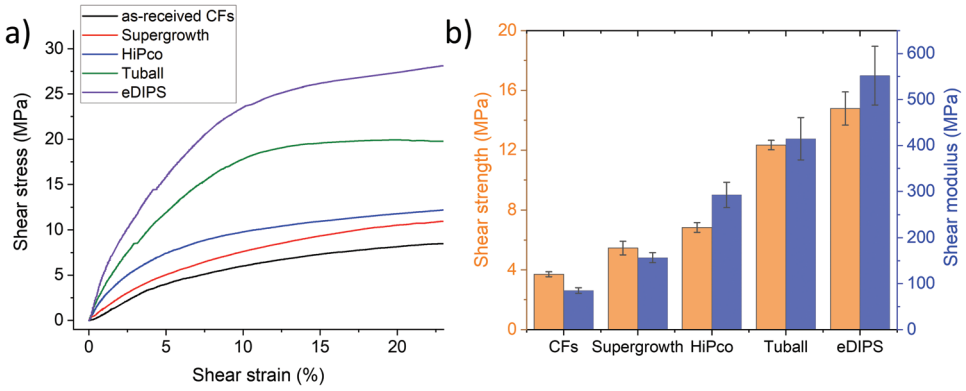

Figure 5. The results of $[\pm 45]_s$ in-plane shear test of CNT-infiltrated CFs infused with PEGDGE/IL-based solid polymer electrolyte: a) typical shear strain versus shear stress curves and b) in-plane shear strength and shear modulus for as-received and CNT-infiltrated CF fabrics.

capacitance value (16.6 F g^{-1}), consistent with their high surface area. However, Supergrowth SWCNTs had lower capacitance when normalized by SSA (85 mF m^{-2}) as compared to the other types of nanotube (140–160 mF m^{-2}). This lower efficiency indicates that not all the surface area measured by gas sorption is available electrochemically to the relatively large ions of the ionic liquid; in this case, likely, the internal pores of the opened Supergrowth tubes do not contribute effectively to capacitance. The area normalized capacitance of the other SWCNTs is similar to the best carbon materials used for EDLCs,[63] reflecting the high electrochemical accessibility of the SWCNT network. The high electrical conductivity of CNT-infiltrated CFs electrodes translates to excellent rate capability; the devices retained 78–83% of their capacitance at up to 100 mA cm^{-2}. The HiPco SWCNT-infiltrated electrodes showed the biggest decline, consistent with the ion diffusion limitations identified in the EIS. The electrochemical performance of the nanotubide infiltrated materials was dramatically higher than that of the bath-sonicated controls, manifested in reduced resistance, larger capacitance, and higher rate capability (Figure S12, Supporting Information).

The values of real energy and power densities were estimated directly from the discharge profiles, with the ohmic drop and non-linear shape of the curves taken into account (Figure 4d). The theoretical energy and power values reported in literature for structural electrodes and supercapacitors are frequently calculated assuming an ideal triangular shape of GCD curves and ignoring the ohmic drop ($E_{max} = \frac{CV^2}{2}$ and $P_{max} = \frac{V^2}{4 * R}$). However, these values in general do not represent practical performance, particularly in systems with higher ESR. By direct measurement, all four devices achieved excellent specific power densities (6.0 kW kg^{-1} for Supergrowth, 8.0 kW kg^{-1} for HiPco, and 8.7 kW kg^{-1} for EDIPS and Tuball, normalized by the total electrode weight, including the CF). The high power performance of CNT-infiltrated CFs normalized to the mass of electrodes, is in the range of values reported for monofunctional non-structural electrodes of conventional supercapacitors (0.5–60 kW kg^{-1}),64,65 which can be attributed to the remarkable electric conductivity induced by deposition of graphitic SWCNTs. The energy densities obtained for SWCNT-infiltrated CFs naturally follow the trend observed for specific capacitance, with the largest value of 4.2 Wh kg^{-1}, at low current densities, recorded for Supergrowth SWCNTs. The maximum energy density values for the other SWCNT-infiltrated fabrics ranged between 2.6 and 3.5 Wh kg^{-1}, in line with the capacitance and surface area trends discussed above. For comparison with approaches in the literature, the maximum theoretical energy and power values of the structural electrodes were also estimated. For the Tuball SWCNT-CF device, the theoretical energy density was calculated as $E_{max} = \frac{CV^2}{2}$, using the actual voltage applied (2.7 V), reaches 3.8 Wh kg^{-1}, when power density ($P_{max} = \frac{V^2}{4 * R}$) is 58 kWg kg^{-1}. The large power density substantially exceeds the values of previously reported structural electrodes, normally found between 0.4–5 kWg kg^{-1} (see Table S7 in Supporting Information). One critical challenge in structural power electrodes is how to transfer mechanical load effectively between the CFs, in the absence of a conventional structural resin. One potential advantage of infiltrating a network of SWCNTs throughout the CF fabric is that it may contribute to the matrix-dominated mechanical properties of the subsequent CF composites. The fiber-dominated tensile properties of the composites are not expected to be significantly affected by the non-damaging, room-temperature infiltration of the nanotubide. Instead, in-plane shear properties were determined to explore whether the SWCNTs offer any matrix reinforcement. A poly(ethylene glycol) diglycidyl ether (PEGDGE)-based structural electrolyte (cross-linked PEGDGE containing 10 wt. % of EMIM TFSI) was utilized as a classic, simple, multifunctional matrix, widely explored in the literature.[6] There is a well-recognized trade-off between matrix stiffness and ionic conductivity that remains a major focus of ongoing work in structural energy storage.[11] As expected, in order to supply useful ionic conductivity, the PEGDGE matrix has lower mechanical performance than conventional epoxies, which translates to lower absolute shear moduli of the composite.[66] However, the PEGDGE matrix does offer sufficient ionic mobility and mechanical stability in multifunctional devices to explore the effects of electrode modifications.

Typical shear stress–strain curves (**Figure 5**a) showed that the presence of SWCNTs has a significant reinforcing effect on the in-plane shear properties of the laminates. The shear strength was improved by 84–400% and the shear modulus was enhanced by 244–549% for different SWCNT materials relative to the as-received CF composite (Figure 5b; Table S3, Supporting Information). The most pronounced increase was observed for long and highly graphitic Tuball (G_{12} = 415 MPa, τ_{12} = 12.3 MPa) and EDIPS (G_{12} = 552 MPa, τ_{12} = 14.8 MPa) SWCNTs. The improved in-plane shear properties after SWCNT infiltration can be attributed to several factors. First, SWCNTs coated on the surface of individual carbon fibers can promote better wetting and adhesion between the matrix and CFs, thus enhancing the stiffness of matrix/fiber interface.[39] This interaction preserves fiber orientation and reduces scissoring of the composite in shear. Secondly, some fraction of CNTs, remaining in the gaps between fibers, may act as a nanoreinforcement providing enhanced matrix-dominated properties, similar to bulk polymer nanocomposites.[67,68] Finally, the compacted SWCNT layer adhered to the surface of the CF fabric may serve as additional reinforcement,[69–71] similar to an isotropic CNTs buckypaper or CNT veil. Once infused to form composite, such materials have significant in-plane mechanical properties and have often been introduced as interlaminar reinforcements in purely structural composites.[72,73]

The variation in textural, mechanical, electrochemical, and conductive properties highlights that multifunctional performance can be tuned through the starting nanocarbon material selection. A parallel coordinate plot provides a useful summary of the multifunctional performance of the SWCNT-infiltrated CFs (Figure S13, Supporting Information). As an example, infiltration of the high surface area and highly defective Supergrowth nanotubes provides the most pronounced enhancement in energy storage performance of the structural hybrid electrode but offers relatively smaller increases in electrical conductivity and mechanical properties. In contrast, infiltration of highly graphitic EDIPS SWCNTs offers the largest increment in conductivity and mechanical reinforcement, but moderate capacitive performance. In the present study, the optimum balance between mechanical and electrochemical properties was achieved by infiltrating Tuball nanotubes. Therefore, a full structural supercapacitor was fabricated using CF fabrics infiltrated with Tuball SWCNTs as electrodes, two glass fiber layers as separators, and a PEGDGE-based polymer electrolyte containing 10 wt.% EMIMTFSI as a simple structural electrolyte.

In-plane tensile tests of these structural supercapacitors confirmed that, as expected, the mild reductive infiltration of the CF fabrics does not significantly affect the mechanical performance in the fiber direction. The stress-strain curves (**Figure 6**a) showed similar behavior for the composites in tension, with similar modulus and tensile strength, both with and without SWCNT infiltration; in both cases, samples failed by delamination caused by the relatively weak polymer matrix used as the structural electrolyte.[27,74] The very large improvement in electrochemical properties, following SWCNT infiltration, which was observed for monofunctional devices, is translated to an increase in energy storage performance of the full structural supercapacitors. Nyquist plots (Figure 6b) showed a reduced ESR from 14.7 to 6.0 kΩcm^2 as a result of introducing the highly conductive nanocarbons. The high resistance of the simple structural electrolyte is reflected in the tilted shape of CV curves (Figure 6c), which becomes more pronounced at higher scan rates (Figure S14a,b, Supporting Information). The specific capacitance (Figure S14c, Supporting Information), determined by integrating the area of CV plots, for as-received and CNT-infiltrated CF-based structural supercapacitors was 7.7 and 34.9 mF g^{-1}, respectively.

The GCD curves (Figure 6d) confirm that the infiltration of SWCNTs into the CF fabrics significantly increased the electrochemical energy stored in the device, observed as a pronounced increase in the area under discharge profile. The values of real energy and power densities calculated by integrating this area reached 1.6 mWh kg^{-1} and 193 mW kg^{-1}, respectively (Figure S14d, Supporting Information). In comparison, the structural device based on as-received CFs alone offered only E_{real} = 0.004 mWh kg^{-1} and P_{real} = 74 mW kg^{-1}. The improvement in capacitance and charge transport provided by the SWCNT-infiltrated fabric architecture allows the real electrochemical performance of structural devices in this work to be directly evaluated by GCD cycling; many previous studies rely only on a "fitted" chronoamperopotential approach, due to unfeasibly long discharge times.[25,27,36,66] Tables S4–S6 in Supporting Information summarise the properties of structural supercapacitors based on as-received CFs and CNT-infiltrated CFs.

The absolute capacitance and energy density of CNT-infiltrated CF-based structural supercapacitors were substantially smaller than for the monofunctional devices. The major constraint, in this case, was high ionic resistance of the structural electrolyte, which limits ion diffusion into the CNT networks. As a result, only a small fraction of large capacitive contribution of SWCNTs measured in the pure ionic liquid electrolyte was exploited in the structural devices.

To demonstrate the prospect for potential enhancement of energy storage properties with an improved structural electrolyte, small amounts of additional IL (1 and 6 wt.% of the total device mass) were added to the composite. This addition significantly improved ESR (3.8 and 1.0 kΩcm,^{2} respectively) and specific capacitance (55 and 101 mF g^{-1}, respectively), which translated to an increase in energy and power densities (Figure S15, Supporting Information).

Multifunctional performance in structural energy storage usually involves trade-offs.[5,17] However, for the structural electrodes produced using SWCNT-infiltrated CFs, the excellent mechanical properties of the CFs are retained, whilst delivering a large improvement in capacitive performance (Figure 6e). Although the absolute performance is low, and limited by the structural electrolyte, this structural electrode system is itself very promising. To estimate potential mass-savings by employing multifunctional structural devices, multifunctional efficiency (η_{MF}) can be considered as a combination of mechanical ($\eta_s = E_{MF}/E_{mono}$) and electrochemical ($\eta_s = \Gamma_{MF}/\Gamma_{mono}$) efficiencies.[17] Even though energy density of the structural supercapacitor is significantly lower than that of monofunctional system, the overall multifunctional efficiency approaches $\eta_s = 1$, relative to the available structural electrolyte matrix. The main challenge to improve both mechanical performance and energy storage of structural power devices remains the structural electrolyte. Whilst this study focuses on the structural electrode,

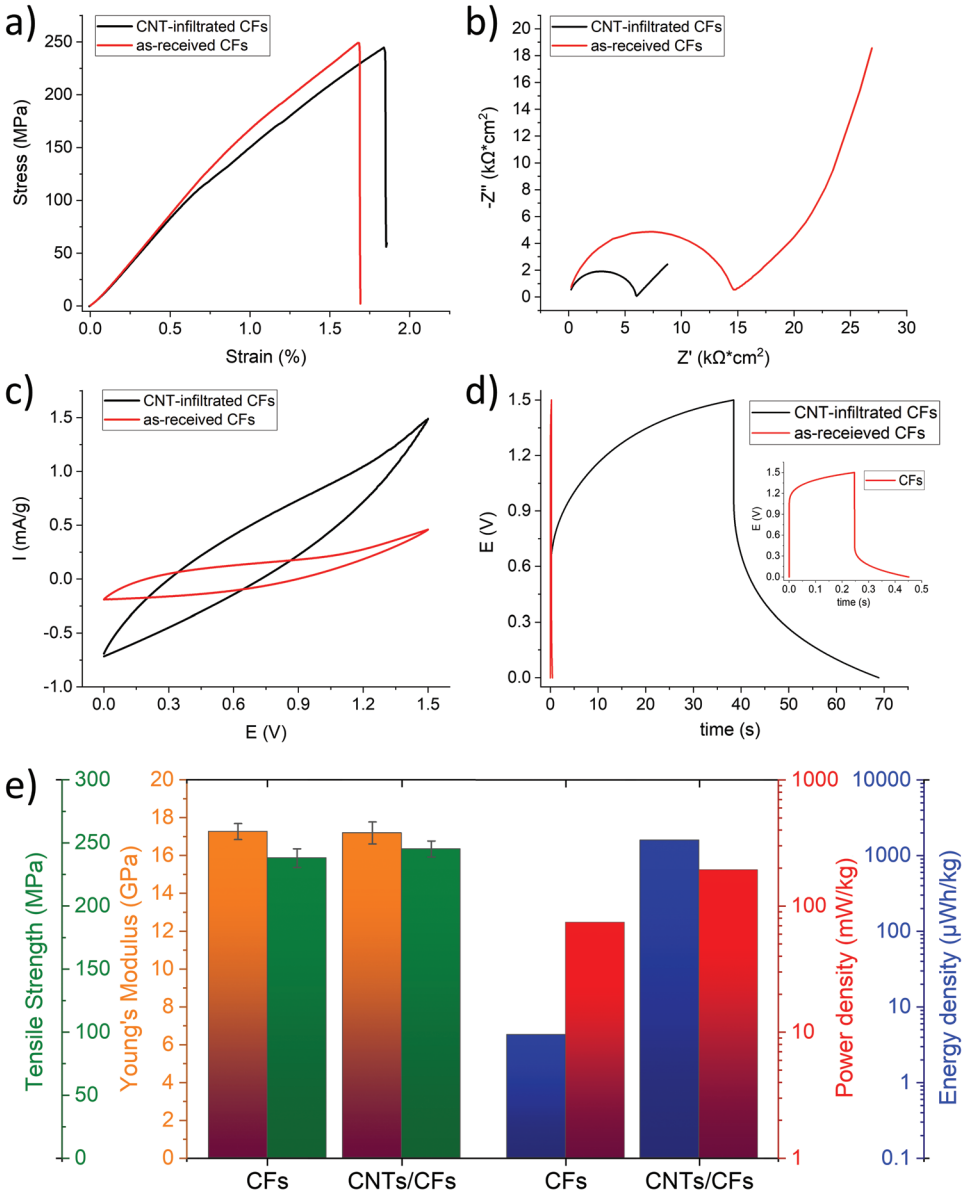

Figure 6. Multifunctional performance of the structural supercapacitors based on as-received CFs and CNT (Tuball)-infiltrated CFs electrodes: a) tensile strain-stress curves, b) Nyquist plots, c) CV curves at 50 mV s^{-1}, d) GCD curves at 40 μA cm^{-2} and e) comparison of tensile strength, Young's modulus, energy, and power densities.

many researchers are working on improving structural electrolytes, particularly exploiting bicontinuous nanostructured systems.[75,76]

It is interesting to compare the mechanical and electrochemical performance of other published works on structural power systems (Table S7 in Supporting Information). However, inconsistency in the methods used both for mechanical and electrochemical characterization of the devices makes a full comparison challenging. Most works report theoretical maximum energy and power values extrapolated from the chronoamperopotential method at low potential. These calculations assume large electrochemical windows are often not achievable for structural supercapacitors; extrapolating a future energy density, using a capacitance derived at low voltages, using $E = \frac{CV^2}{2}$ with a voltage exceeding commercial devices is likely misleading, even more so, if considering pseudocapacitive hybrids.[77] In this work, electrochemical properties represent real performance of the system obtained through the type of GCD cycling applied for conventional energy storage devices. CFs modified through infiltration of charged dispersion of SWCNTs offer both promising structural properties comparable to other studies and energy storage characteristics that surpass those obtained for many multifunctional structural supercapacitors.

3. Conclusions

This work introduces a new approach to infiltrate graphitic SWCNTs into woven CF fabrics using reductively dissolved nanocarbons processed at room temperature. The efficacy of the reductive dissolution approach produces pure buckypapers with exceptional properties ($\sigma \approx 2000$ S cm^{-1}, SSA >1000 m^2 g^{-1} and C ≈100 F g^{-1}) and allows the effective infiltration of SWCNTs into spread tow fiber preforms. The resulting highly porous SWCNT networks are distributed throughout the internal volume of the CF fabrics as a uniform thin (submicron) surface coating. The resulting structural electrodes exhibit exceptional multifunctional performance combining high electrical conductivity, high specific surface area, and enhancements in in-plane shear properties, with only marginal increases in the mass and volume of the fabric. The approach is versatile and was successfully applied to four different nanotube feedstocks, demonstrating the ability to tune the multifunctional performance. In all cases, the SWCNTs synergistically improve both electrochemical and mechanical matrix shear properties. The intrinsic capacitive performance of CNT-infiltrated CFs in ionic liquid is excellent (E = 2.6–4.2 Wh kg^{-1} and P = 6.0–8.7 kW kg^{-1}) and translates to a substantial improvement of energy storage properties of structural supercapacitors, even using a simple structural electrolyte. The values of real energy and power densities for multifunctional structural power devices produced with CNT-modified CFs electrodes are 400 and 2.6 times larger, respectively than those obtained for bare CFs-based structural systems. Taking advantage of the excellent multifunctional performance of the electrode material, the resulting structural supercapacitors can be charged at conditions similar to conventional monofunctional supercapacitors. This realistic testing regime is a significant step, often overlooked in the field, which brings the concept of structural power devices closer to actual application. Unlike other thermal methods, the infiltration of charged nanotubide dispersion does not cause any deterioration of mechanical properties of the material and the laminates demonstrate similar in-plane elastic modulus and tensile strength to those of the control CF-based composite. The key requirement to access the full potential of these structural electrodes is the development of new structural electrolytes, with high ion mobility and mechanical modulus[76,78]; this challenge is central to a wide range of structural power embodiments and is a focus of research worldwide. The SWCNT-CF hybrids presented here could be developed further, using a wide range of other nanomaterial feedstocks and associated optimized reduction protocols. In principle, the performance of different SWCNT feedstocks could be improved by adjusting the dissolution process to remove impurities or to maximize coulombic repulsion (and hence the extent of individualization).[44,47] Although the nanotube concentration and charging ratio were fixed for all nanotubide dispersions in this work, the exact values can affect SWCNTs dispersion/individualization significantly and, consequently, electrochemical properties of capacitor electrodes.[44] The optimal charging ratio can significantly alter for different types of CNTs depending on their specific structural characteristics. In addition to their use in structural supercapacitors, these hybrid infiltrated fabrics have other potential applications in catalyst supports, fuel cell electrodes, and pure structural composites.

Supporting Information

Supporting Information is available from the Wiley Online Library or from the author.

Acknowledgements

Financial support is acknowledged from the funding provided by the EPSRC Future Composites Research Manufacturing Hub (EP/P006701/1), the EPSRC Beyond Structural project (EP/P007465/1), the European Office of Aerospace Research and Development (IOE Grant FA9550-17-1-0251), EU Clean Sky 2 (SORCERER Project #738085) and the Royal Academy of Engineering (Chair in Emerging Technologies). The authors also would like to thank Prof. Kenji Hata and his research group at The National Institute of Advanced Industrial Science and Technology in Japan (AIST), for providing the Supergrowth SWCNTs.

Conflict of Interest

The authors declare no conflict of interest.

Data Availability Statement

The data that support the findings of this study are available from the corresponding author upon reasonable request.

Keywords

carbon nanotubes (CNTs), carbon fiber reinforced polymers (CFRPs), multifunctional structural supercapacitors, nanotubide, reductive dissolution

Received: November 1, 2022
Revised: January 11, 2023
Published online:

[1] M. J. Nieuwenhuijsen, *Environ. Int.* **2020**, *140*, 105661.
[2] E. Karadotcheva, S. N. Nguyen, E. S. Greenhalgh, M. S. P. Shaffer, A. R. J. Kucernak, P. Linde, *Energies* **2021**, *14*, 6006.
[3] K. Turcheniuk, D. Bondarev, V. Singhal, G. Yushin, **2018**.
[4] H. Zhou, H. Li, L. Li, T. Liu, G. Chen, Y. Zhu, L. Zhou, H. Huang, *Mater. Today Energy* **2022**, *24*, 100924.
[5] J. F. Snyder, E. B. Gienger, E. D. Wetzel, *J. Compos. Mater.* **2015**, *49*, 1835.
[6] Y. Xu, W. Lu, G. Xu, T.-W. Chou, *Compos. Sci. Technol.* **2021**, *204*, 108636.
[7] L. E. Asp, K. Bouton, D. Carlstedt, S. Duan, R. Harnden, W. Johannisson, M. Johansen, M. K. G. Johansson, G. Lindbergh, F. Liu, *Adv. Energy Sustain. Res.* **2021**, *2*, 2000093.
[8] L. E. Asp, M. Johansson, G. Lindbergh, J. Xu, D. Zenkert, *Funct. Compos. Struct.* **2019**, *1*, 042001.
[9] S. Ekstedt, M. Wysocki, L. E. Asp, *Plast. rubber Compos.* **2010**, *39*, 148.
[10] P. Liu, E. Sherman, A. Jacobsen, *J. Power Sources* **2009**, *189*, 646.
[11] L. E. Asp, E. S. Greenhalgh, *Compos. Sci. Technol.* **2014**, *101*, 41.
[12] X. Luo, D. D. L. Chung, *Compos. Sci. Technol.* **2001**, *61*, 885.
[13] Y. Xu, W. Lu, G. Xu, T.-W. Chou, *Compos. Sci. Technol.* **2020**, 108636.
[14] T. Carlson, L. Asp, *J. Multifunct. Compos.* **2013**, *1*, 91.
[15] T. Carlson, D. Ordéus, M. Wysocki, L. E. Asp, *Compos. Sci. Technol.* **2010**, *70*, 1135.

[16] K.-Y. Chan, A. Baktash, B. Demir, E. L. H. Mayes, D. Yang, D. Q. Pham, K.-T. Lin, A. P. Mouritz, A. S. M. Ang, B. Fox, *J. Power Sources* **2021**, *482*, 229020.
[17] D. J. O'Brien, D. M. Baechle, E. D. Wetzel, *J. Compos. Mater.* **2011**, *45*, 2797.
[18] C. D. Hilton, D. M. Peairs, J. J. Lesko, S. W. Case, *J. Fuel Cell Sci. Technol.* **2011**, *8*, 51008.
[19] E. D. Wetzel, *AMPTIAC Q* **2004**, *8*, 91.
[20] H. Dai, E. T. Thostenson, *Carbon N. Y.* **2020**, *164*, 28.
[21] J. C. Fernández-Toribio, A. Íñiguez-Rábago, J. Vilà, C. González, Á. Ridruejo, J. J. Vilatela, *Adv. Funct. Mater.* **2016**, *26*, 7139.
[22] A. Alsaadi, Y. Shi, L. Pan, J. Tao, Y. Jia, *Compos. Sci. Technol.* **2019**, *178*, 1.
[23] W. Johannisson, *Ph.D. dissertation*, KTH Royal Institute of Technology (Stockholm) **2020**.
[24] W. Johannisson, R. Harnden, D. Zenkert, G. Lindbergh, *Proc. Natl. Acad. Sci* **2020**, *117*, 7658.
[25] H. Qian, A. R. Kucernak, E. S. Greenhalgh, A. Bismarck, M. S. P. Shaffer, *ACS Appl. Mater. Interfaces* **2013**, *5*, 6113.
[26] E. Senokos, Y. Ou, J. J. Torres, F. Sket, C. González, R. Marcilla, J. J. Vilatela, *Sci. Rep.* **2018**, *8*, 3407.
[27] A. Ganguly, A. Karakassides, J. Benson, S. Hussain, P. Papakonstantinou, *ACS Appl. Energy Mater.* **2020**, *3*, 4245.
[28] T. Ma, H. Yang, L. Lu, *Appl. Energy* **2015**, *153*, 56.
[29] H. Guentri, T. Allaoui, M. Mekki, M. Denai, *J. Energy Storage* **2021**, *39*, 102578.
[30] A. M. Navarro-Suárez, M. S. P. Shaffer, *Front. Chem.* **2022**, *9*, 810781.
[31] E. Fitzer, L. M. Manocha, *Carbon reinforcements and carbon/carbon composites*, Springer Science & Business Media, Berlin **1998**.
[32] E. Savage, *Carbon-carbon composites*, Springer Science & Business Media, Berlin **2012**.
[33] L. Shen, Q. Che, H. Li, X. Zhang, *Adv. Funct. Mater.* **2014**, *24*, 2630.
[34] A. Mishra, N. Shetti, S. Basu, K. Reddy, T. Aminabhavi, *ChemElectroChem* **2019**, *6*, 5771.
[35] H. Qian, H. Diao, N. Shirshova, E. S. Greenhalgh, J. G. H. Steinke, M. S. P. Shaffer, A. Bismarck, *J. Colloid Interface Sci.* **2013**, *395*, 241.
[36] N. Shirshova, H. Qian, M. Houllé, J. H. G. Steinke, A. R. J. Kucernak, Q. P. V. Fontana, E. S. Greenhalgh, A. Bismarck, M. S. P. Shaffer, *Faraday Discuss.* **2014**, *44*, 81.
[37] B. K. Deka, A. Hazarika, J. Kim, N. Kim, H. E. Jeong, Y.-B. Park, H. W. Park, *Chem. Eng. J.* **2019**, *355*, 551.
[38] B. K. Deka, A. Hazarika, J. Kim, Y.-B. Park, H. W. Park, *Compos. Part A Appl. Sci. Manuf.* **2016**, *87*, 256.
[39] H. Qian, A. Bismarck, E. S. Greenhalgh, M. S. P. Shaffer, *Compos. Part A Appl. Sci. Manuf.* **2010**, *41*, 1107.
[40] X. F. Sánchez-Romate, A. Del Bosque, J. Artigas-Arnaudas, B. K. Muñoz, M. Sánchez, A. Ureña, *Electrochim. Acta* **2021**, *370*, 137746.
[41] A. J. Clancy, M. K. Bayazit, S. A. Hodge, N. T. Skipper, C. A. Howard, M. S. P. Shaffer, *Chem. Rev.* **2018**, *118*, 7363.
[42] A. J. Clancy, D. B. Anthony, S. J. Fisher, H. S. Leese, C. S. Roberts, M. S. P. Shaffer, *Nanoscale* **2017**, *9*, 8764.
[43] M. De Marco, F. Markoulidis, R. Menzel, S. M. Bawaked, M. Mokhtar, S. A. Al-Thabaiti, S. N. Basahel, M. S. P. Shaffer, *J. Mater. Chem. A* **2016**, *4*, 5385.
[44] P. Sirisinudomkit, E. Senokos, N. Rubio, M. S. P. Shaffer, *Mater. Adv.* **2021**, *2*, 1981.
[45] A. J. Clancy, H. Au, N. Rubio, G. O. Coulter, M. S. P. Shaffer, *Dalt. Trans.* **2020**, *49*, 10308.
[46] H. S. Leese, L. Govada, E. Saridakis, S. Khurshid, R. Menzel, T. Morishita, A. J. Clancy, E. R. White, N. E. Chayen, M. S. P. Shaffer, *Chem. Sci.* **2016**, *7*, 2916.
[47] A. J. Clancy, J. Melbourne, M. S. P. Shaffer, *J. Mater. Chem. A* **2015**, *3*, 16708.
[48] M. C. G. Santos, D. R. da Silva, P. S. Pinto, A. S. Ferlauto, R. G. Lacerda, W. P. Jesus, T. H. R. da Cunha, P. F. R. Ortega, R. L. Lavall, *Electrochim. Acta* **2020**, *349*, 136241.
[49] J. Che, P. Chen, M. B. Chan-Park, *J. Mater. Chem. A* **2013**, *1*, 4057.
[50] Q. Yin, H. Jia, G. Liu, Q. Ji, *Adv. Funct. Mater.* **2022**, *32*, 2111177.
[51] Q. Yin, M. Ye, H. Jia, A. F. A. de Araújo Melo, Q. Ji, *J. Mater. Chem. A.* **2022**, *10*, 21430
[52] H. D. Asfaw, A. Kucernak, E. S. Greenhalgh, M. S. P. Shaffer, (under revision), **2022**.
[53] T. R. Pozegic, J. V. Anguita, I. Hamerton, K. D. G. I. Jayawardena, J.-S. Chen, V. Stolojan, P. Ballocchi, R. Walsh, S. R. P. Silva, *Sci. Rep.* **2016**, *6*, 37334.
[54] H. Okuda, R. J. Young, D. Wolverson, F. Tanaka, G. Yamamoto, T. Okabe, *Carbon N. Y.* **2018**, *130*, 178.
[55] M. A. Montes-Morán, R. J. Young, *Carbon N. Y.* **2002**, *40*, 845.
[56] F. Tuinstra, J. Lo Koenig, *J. Chem. Phys.* **1970**, *53*, 1126.
[57] M. F. Pernice, G. Qi, E. Senokos, D. B. Anthony, S. Nguyen, M. Valkova, E. S. Greenhalgh, M. S. P. Shaffer, A. R. J. Kucernak, *Multifunct. Mater.* **2022**, *5*, 025002.
[58] O. Kimizuka, O. Tanaike, J. Yamashita, T. Hiraoka, D. N. Futaba, K. Hata, K. Machida, S. Suematsu, K. Tamamitsu, S. Saeki, Y. Yamada, H. Hatori, *Carbon N. Y.* **2008**, *46*, 1999.
[59] S. Ilani, L. A. K. Donev, M. Kindermann, P. L. McEuen, *Nat. Phys.* **2006**, *2*, 687.
[60] E. Senokos, *Ph.D. Thesis*, Universidad Politécnica de Madrid, **2018**.
[61] D. Pech, M. Brunet, H. Durou, P. Huang, V. Mochalin, Y. Gogotsi, P.-L. Taberna, P. Simon, *Nat. Nanotechnol.* **2010**, *5*, 651.
[62] N. Díez, R. Mysyk, W. Zhang, E. Goikolea, D. Carriazo, *J. Mater. Chem. A* **2017**, *5*, 14619.
[63] H. Ji, X. Zhao, Z. Qiao, J. Jung, Y. Zhu, Y. Lu, L. L. Zhang, A. H. MacDonald, R. S. Ruoff, *Nat. Commun.* **2014**, *5*, 3317.
[64] W. Raza, F. Ali, N. Raza, Y. Luo, K.-H. Kim, J. Yang, S. Kumar, A. Mehmood, E. E. Kwon, *Nano Energy* **2018**, *52*, 441.
[65] A. Borenstein, O. Hanna, R. Attias, S. Luski, T. Brousse, D. Aurbach, *J. Mater. Chem. A* **2017**, *5*, 12653.
[66] N. Shirshova, H. Qian, M. S. P. Shaffer, J. H. G. Steinke, E. S. Greenhalgh, P. T. Curtis, A. Kucernak, A. Bismarck, *Compos. Part A Appl. Sci. Manuf.* **2013**, *46*, 96.
[67] H. Qian, E. S. Greenhalgh, M. S. P. Shaffer, A. Bismarck, *J. Mater. Chem.* **2010**, *20*, 4751.
[68] A. K. Subramaniyan, C. T. Sun, *Compos. Part A Appl. Sci. Manuf.* **2006**, *37*, 2257.
[69] N. Li, G. dong Wang, S. K. Melly, T. Peng, Y. C. Li, Q. Di Zhao, S. de Ji, *Compos. Struct.* **2019**, *208*, 13.
[70] H. Kim, *Met. Mater. Int.* **2015**, *21*, 185.
[71] Y. Wu, X. Cheng, S. Chen, B. Qu, R. Wang, D. Zhuo, L. Wu, *Mater. Des.* **2021**, *202*, 109535.
[72] Y. Ou, C. González, J. J. Vilatela, *Compos. Part B Eng.* **2020**, *201*, 108372.
[73] Y. Ou, C. González, J. J. Vilatela, *Compos. Part A Appl. Sci. Manuf.* **2019**, *124*, 105477.
[74] Z. Sha, F. Huang, Y. Zhou, J. Zhang, S. Wu, J. Chen, S. A. Brown, S. Peng, Z. Han, C.-H. Wang, *Compos. Sci. Technol.* **2021**, *201*, 108568.
[75] L. M. Schneider, N. Ihrner, D. Zenkert, M. Johansson, *ACS Appl. Energy Mater.* **2019**, *2*, 4362.
[76] V. Tu, L. E. Asp, N. Shirshova, F. Larsson, K. Runesson, R. Jänicke, *Multifunct. Mater.* **2020**, *3*, 025001.
[77] T. S. Mathis, N. Kurra, X. Wang, D. Pinto, P. Simon, Y. Gogotsi, *Adv. Energy Mater.* **2019**, *9*, 1902007.
[78] C. Lee, E. S. Greenhalgh, M. S. P. Shaffer, A. Panesar, *Multifunct. Mater.* **2019**, *2*, 045001.